High Precision GPS Measurements

AFOSR grant # FA9550-07-1-0354
AFOSR Program: Test and Evaluation
Project Duration: 03/01/07-11/30/09
Program Manager: Dr. Jon Sjogren

Principal Investigator: Y. Morton
Department of Electrical and Computer Engineering
Miami University
Oxford, OH

Co-Principal Investigator: F. van Graas
School of Electrical Engineering and Computer Science
Ohio University
Athens, OH

Final Report Table of Content

REPORT DOCUMENTATION PAGE

Form Approved
OMB No. 0704-0188

1. REPORT DATE *(DD-MM-YYYY)*	**2. REPORT TYPE**	**3. DATES COVERED** *(From - To)*
02/28/10	Final report	03/01/2007-11/30/2009

4. **TITLE AND SUBTITLE**
High Precision GPS Measurements

5a. CONTRACT NUMBER
FA9550-07-1-0354

5b. GRANT NUMBER

5c. PROGRAM ELEMENT NUMBER

6. AUTHOR(S)
Y. Morton, F. van Graas

5d. PROJECT NUMBER

5e. TASK NUMBER

5f. WORK UNIT NUMBER

7. PERFORMING ORGANIZATION NAME(S) AND ADDRESS(ES)

Miami University
7 Roudebush Hall
Oxford, OH 45056-3563

8. PERFORMING ORGANIZATION REPORT NUMBER

9. SPONSORING / MONITORING AGENCY NAME(S) AND ADDRESS(ES)
USAF, AFRL
AFOSR
875 North Randolph St.
Suite 325, Room 3112
Arlington, VA 22203

10. SPONSOR/MONITOR'S ACRONYM(S)
AFOSR

11. SPONSOR/MONITOR'S REPORT NUMBER(S)
AFRL-SR-AR-TR-10-0158

12. DISTRIBUTION / AVAILABILITY STATEMENT
Distribution A: Approved for Public Release

13. SUPPLEMENTARY NOTES
N/A

14. ABSTRACT

The objective of this project is to develop high precision GPS receivers by utilizing modernized GPS signals at L1, L2, and L5 frequencies to mitigate GPS measurement errors. For each successfully acquired and tracked GPS signal, a GPS receiver generates two receiver-satellite range observables: the code phase and the carrier phase measurements. Precision GPS solutions are obtained by exploiting both observables at all available frequencies to eliminate, reduce, or estimate various error sources. These error sources include signal propagation errors through the ionosphere and troposphere, satellite orbit and clock errors, receiver clock error, receiver noise, multipath error, hardware bias, and integer cycle ambiguities associated with the carrier phase observables. The project proposed an array of innovative methods to assess and mitigate these errors. Since the start of the project in March 2007, we made significant progress in three major areas: (a) Higher order ionosphere error temporal and spatial variations studies; (b) satellite orbit and clock error characterization; (c) modeling of troposphere error under severe weather conditions. The report summarizes the progress made in these three areas.

15. SUBJECT TERMS

16. SECURITY CLASSIFICATION OF: Unclassified			**17. LIMITATION OF ABSTRACT**	**18. NUMBER OF PAGES**	**19a. NAME OF RESPONSIBLE PERSON**
a. REPORT	**b. ABSTRACT**	**c. THIS PAGE**		3	Y. T. Jade Morton
					19b. TELEPHONE NUMBER *(include area code)* 513-529-0749

1. Technical Summary

The objective of this project is to develop high precision GPS receivers by utilizing modernized GPS signals at L1, L2, and L5 frequencies to mitigate GPS measurement errors. For each successfully acquired and tracked GPS signal, a GPS receiver generates two receiver-satellite range observables: the code phase and the carrier phase measurements. Precision GPS solutions are obtained by exploiting both observables at all available frequencies to eliminate, reduce, or estimate various error sources. These error sources include signal propagation errors through the ionosphere and troposphere, satellite orbit and clock errors, receiver clock error, receiver noise, multipath error, hardware bias, and integer cycle ambiguities associated with the carrier phase observables. The project proposed an array of innovative methods to assess and mitigate these errors. Since the start of the project in March 2007, we made significant progress in three major areas: (a). Higher order ionosphere error temporal and spatial variations studies; (b). satellite orbit and clock error characterization; (c) modeling of troposphere error under severe weather conditions. The following summarizes the background and progress made in these three areas.

1.1. Higher order ionosphere error temporal and spatial variation studies.

The ionosphere can be approximated as a collision-less cold plasma bathed in the geomagnetic field. Such magnetically biased plasma interacts with propagating electromagnetic waves. The result is manifested in the non-unity refractive index whose values are determined by the electron density distributions and the projection of the geomagnetic fields along the signal propagation direction. The non-unity refractive index causes signal group delay and carrier phase advances. The high variability and unpredictability of the ionosphere made the ionosphere propagation error the most dominant error source in GPS range measurements, ranging from a few meters to tens of meter under quiet solar conditions to hundreds of meters during geomagnetic storms [1]. Based on the classical magneto-ionic theory, the ionosphere code and carrier errors are approximated as the sum of first, second, and third order terms proportional to $1/f^2$, $1/f^3$, $1/f^4$ respectively [2]. The first order error is the dominant term and it is only dependent on the total electron content (TEC) along the signal propagation path. The second and third order errors are typically a few cm and sub-mm, respectively. They both depend on electron density and magnetic field vector distributions along the signal propagation path. During solar maximum and geomagnetically active periods, the third order error may become comparable with the second order error, reaching the 10's of cm level.

Despite the dominant nature of the first order ionosphere error, it can be eliminated by range measurements from two frequencies using a dual-frequency receiver. The second and third order errors remain in the receiver error budget and have not received much attention until recently. For high accuracy applications such as reference systems, surveying, plate tectonic motion, crustal deformation and atmospheric sounding, low earth orbit (LEO) satellite radio occultation measurements, and imaging sensor platform precise position and navigation, the higher order errors become important error factors [3][4]. Studies of the higher order errors are challenging because they require accurate knowledge of the ionosphere parameter distributions. Prior studies of higher order error are based on simplified ionosphere models [5][6][7]. There is a lack of understanding of both their temporal and spatial structures which are critical to development of error mitigation techniques.

In this project, we took a unique approach in applying the Appleton-Hartree formula [8] to the computation of the higher order errors by combining vertical electron density profiles obtained from the Arecibo incoherent scatter radar (ISR) and the International Reference Ionosphere (IRI) model, TEC maps derived from the International GNSS Service (IGS) database, and magnetic field vectors from the International Geomagnetic Reference Field (IGRF) model [9]. These combined measurements and models allow us to compute the second and third order errors at a given geodetic location and time for signals arriving from arbitrary directions. The 24-slot GPS baseline constellation is used to compute a receiver position error based on higher order range error [10]. Major accomplishments achieved on this area of the project to date are:

(1) *ISR measured electron density profiles and IGRF models for higher order error computation.*

We obtained multi-years ISR electron density measurements at three strategic sites: Millstone Hill, MA, Arecibo, Puerto Rico, and Jicamarca, Peru. Using data from these three sites allow us to characterize the geographical dependency of the ionosphere higher order error. Table 1 lists the geographical and data parameters associated with each of the sites. Fig. 1 shows example electron density profiles from these three sites. The data covered nearly every hour of a day, every month in a year, and a wide range of solar-geomagnetic conditions for a typical low latitude location.

Table 1: ISR site and data information

	Millstone Hill Observatory	Arecibo Observatory	Jicamarca Radio Observatory
Location	Westford, Massachusetts	Puerto Rico	Lima, Peru
North Latitude	42° 37′ 10″	18° 20′ 36.6″	−11° 57′ 5″
East Longitude	288° 30′ 29″	293° 14′ 48.9″	283° 7′ 48″
Altitude ASL	146 m	497 m	520 m
Magnetic Latitude	52.89 deg	28.65 deg	-1.46 deg
Magnetic Longitude	0.10 deg	5.22 deg	354.81 deg
Altitude range	100 km – 548 km	56 km – 500 km	59 km – 1635 km
Altitude resolution	14 km	600 m	15 km
Time resolution	15 min	1 min	10 min
Dates of data used	4/16/2002 – 5/14/2009	9/23/1986 – 4/15/2000	8/13/2002 – 4/26/2009
No. days Kp < 5	273	225	76
No. days Kp ≥ 5	26	39	1

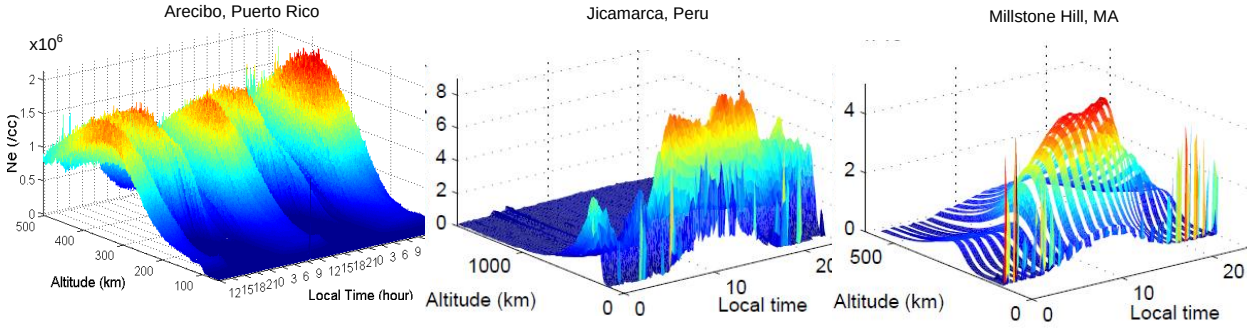

Fig. 1. Example electron density profiles measured by ISRs at three locations under study.

The values of the magnetic field vector were determined by the 10th generation IGRF model. The IGRF has traditionally been fitted to data from ground-based magnetic observatories. Although the 10th generation has been based upon data obtained from satellites, its applicability to the upper atmosphere might remain questionable. To address this, we analyzed over one

decade of ionospheric magnetometer field measurements from low Earth orbiting satellites. As part of the International Decade of Geopotential Field Research, several satellites carrying magnetometers were launched. We used results from SAC-C, CHAMP, and Orsted. We found that the IGRF model accurately represents the ionospheric magnetic field. The mean variation of the measurements from the model was less than 60 nT everywhere, which is less than 0.2% of the average ionospheric field strength of 35,541 nT. 99.58% of the measurements were within 0.5% of the model. The standard deviation of measurements about the IGRF was 40.7 nT. Fig. 2 plots the mean absolute difference between the model and over 600GB of measurement data from the three satellites collected during nearly one decade. Detailed analysis of the IGRF performance in modeling the magnetic field in the ionosphere is in revision for publication [11].

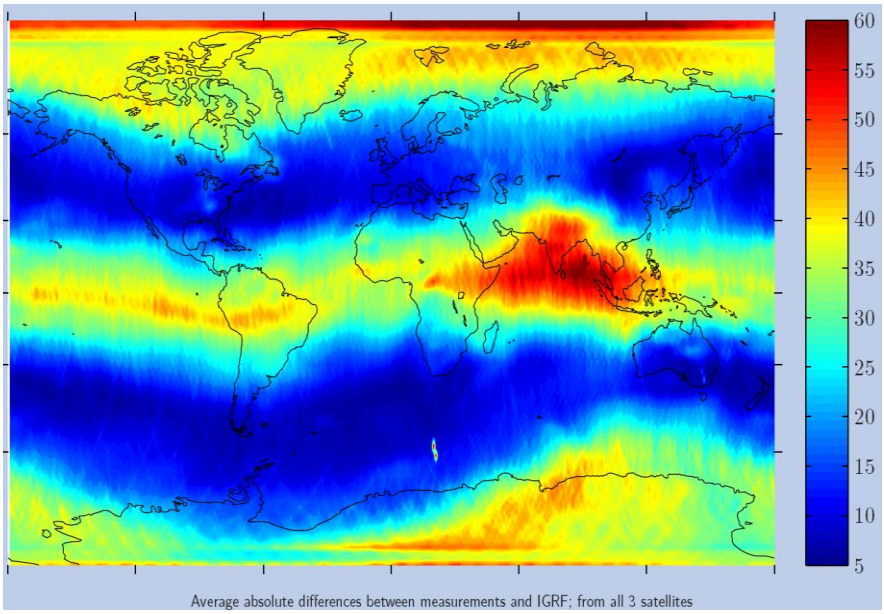

Fig. 2. Absolute mean difference between IGRF model and satellite measurements (nT).

(2) *Higher order error temporal behavior*.

The extensive Arecibo ISR data and validation of the IGRF model allowed us to obtain comprehensive understanding of the daily, seasonal, and solar cycle behavior of the higher order error. Fig. 3 shows the second order error diurnal variation pattern for signals arriving from zenith, south at 10^{o} elevation, north at 10^{o} elevation at the three locations. The green and red dots are the sum of second and third order errors computed using each available electron density profile under quiet and active geomagnetic conditions respectively. The blue lines indicate mean and standard deviation. These plots clearly show the temporal trend and magnitude of the higher order error for a limited number of directions of arrival.

Additonal correlations between the higher order range error and geomagnetic activity and seasonal variations are also obtained. Fig. 4 shows that the mean and standard deviation of the higher order errors under geomagnetically active and quiet conditions at two of the sites. There is a clear correlation between the geomagnetic activity and enhanced higher order error at both sites.

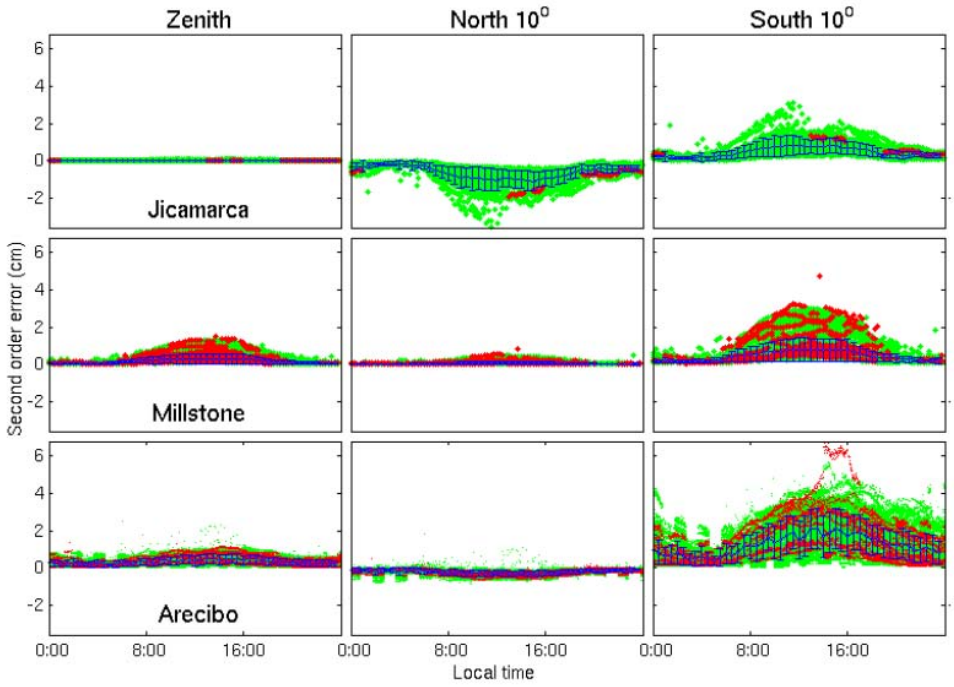

Fig.3. Higher order errors for three directions of signal arrival.

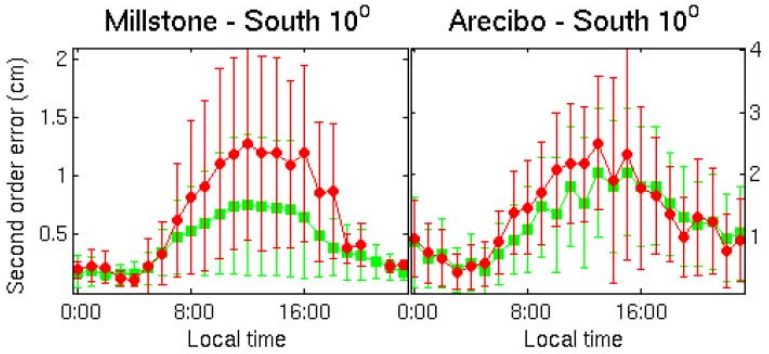

Fig. 4. Mean and standard deviation of higher order error under geomagnetically active (red) and quiet (green) conditions.

The large extensive data sets used in the study also allowed us to obtain an understanding of the higher order error's seasonal variation. Fig. 5 plots the higher order errors in groups of three month each for signals arriving from 10° south at the three ISR sites. Clearly, the higher order error is most prominent during October-December at all three sites.

More details on the temporal behavior of the higher order errors at the three locations can be found in [12].

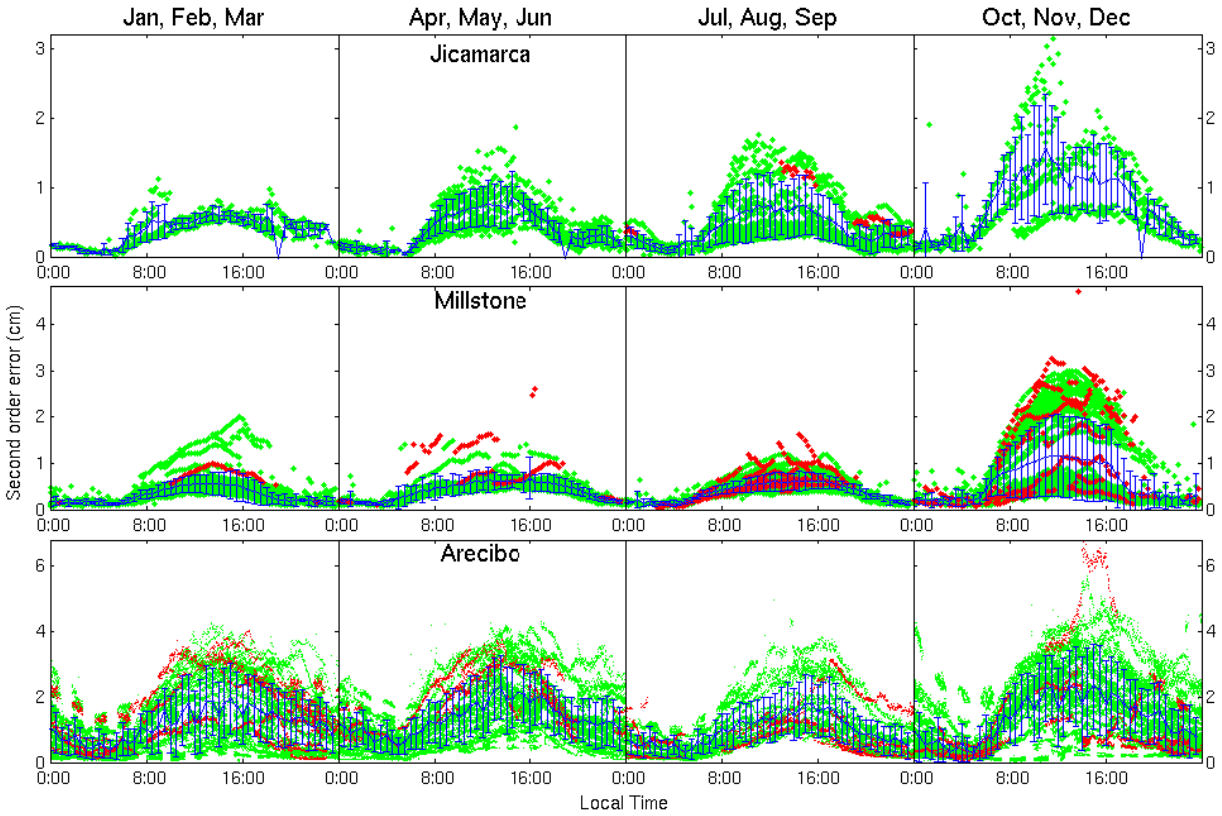

Fig. 5. Seasonal variations of the higher order error at the three ISR sites.

(3) *Higher order error spatial behavior.*

The second order error is fundamentally due to the existence of the geomagnetic field which causes rotations of GPS signal polarizations. A major misunderstanding by prior researchers is that GPS signals can only propagate in the "X" mode because it is right hand circular polarized [13]. A thorough review of the magneto-ionic theory and derivation of the GPS signal polarization demonstrates that GPS signals propagate in both "X" and "O" mode, depending on the signal propagation direction relative to the magnetic field direction [14]. As a result, the second order error can be positive or negative; indicating that the first order error may be an under-estimation or over-estimation. Based on this new derivation, we computed the second order error for signals arriving from all possible directions at the three sites. Fig. 6 provides sky plots that show snap shots of the spatial distribution of the error at the three sites under quiet conditions. The black thick lines at Arecibo and Jicamarca indicate where zero higher order errors occur. Jicamarca is located near the geomagnetic equator. Signals arriving from zenith or along the east-west directions are nearly perpendicular to the magnetic field lines. This is demonstrated by the zero error line shown in the Jicamarca sky

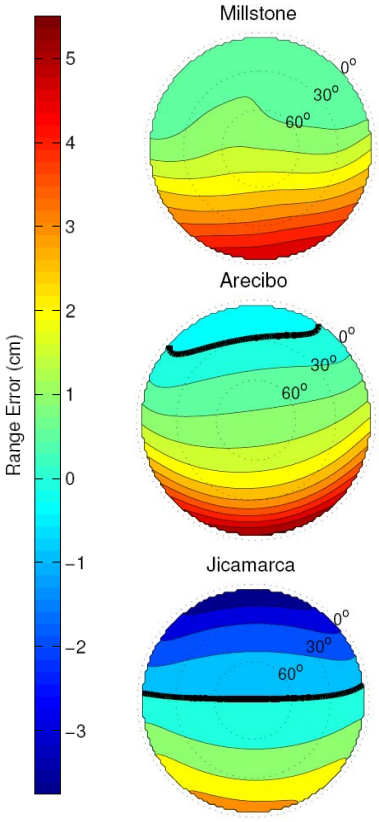

Fig. 6. Eample sky plots of higher order errors

plot. At Millstone, because of the relative high dip angle of the magnetic field, no signal direction arrivals are perpendicular to the magnetic field line, and hence, the lack of zero higher order error occurrence.

(4) *Higher order range error induced position error*.

The ionosphere higher order observable errors directly translate into receiver position errors. We used the 24-slot baseline GPS constellations to evaluate the position error over a 24-hour time period and computed the receiver position error by injecting a higher order error into the range measurements. Fig. 7 is an example plot of the position error over the 24-hour period, assuming the baseline constellation with two possible satellites failure. The receiver location is at Arecibo, Puerto Rico (latitude 18°20'N, longitude 66°45'W). The most prominent position error component is the southward bias in the top panel of the plot.

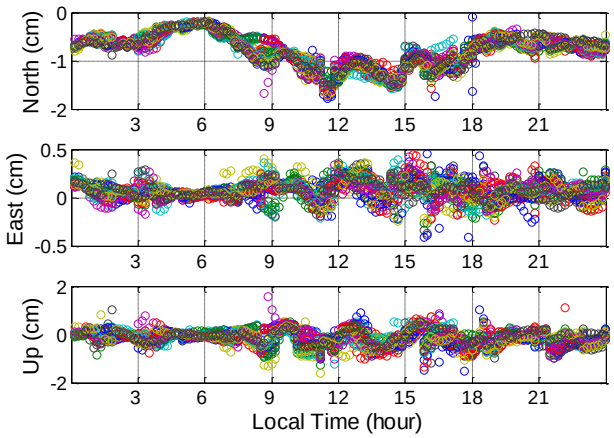

Fig. 7. Higher order error induced receiver position error at Arecibo on a quiet day assuming the 24-slot baseline GPS constellations with 2 possible satellite failures.

We further evaluated the impact of GPS signal propagation mode on position errors. Such impact is obviously location dependent. We selected three sites that are characteristic representations of low-mid latitude northern hemisphere, magnetic equatorial, and low-mid latitude southern hemisphere locations. Jicamarca, Peru is at 1° south of magnetic equator, while Arecibo, Puerto Rico and Bahia Blanca, Argentina are corresponding magnetic conjugate points at northern and southern hemispheres. Fig. 8 shows the locations of the three sites over gridlines of geomagnetic latitude and longitude.

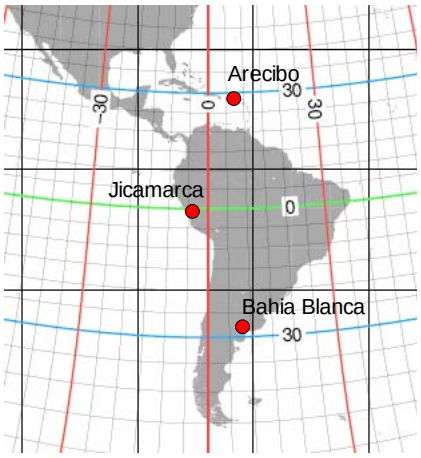

Fig. 8. Locations of three selected sites for second order ionosphere error studies. The grid lines are geomagnetic latitude and longitude lines.

We compute and contrast the receiver position errors due to second order carrier range errors when only the "X" mode is considered and when both "O" and "X" modes are considered. The second order errors are computed based on vertical electron density profiles measured by the Arecibo incoherent scatter radar (ISR) and International Geomagnetic Reference Field (IGRF) model. For signals arriving at arbitrary directions and at other locations, we applied the IGS TEC map to scale the Arecibo ISR profiles [10]. The position errors are computed for the baseline 24-satellite configuration over a 24-hour period in 10 minute intervals. Fig. 9 shows

the position error in receiver local coordinate at the three locations indicated in Fig. 8. This results show that for carrier phase-based dual-frequency receivers where only the first order error is eliminated, the residual second order error will result in a southward bias regardless of the location of the receiver. If an attempt is made to mitigate the second order error, but only the "X" mode of propagation is considered, the consequence will be different depending on the location of the receiver. If a receiver is located in the northern hemisphere, it is most likely that the correction will account for a large portion of the second order error. For a receiver located near the magnetic equator, such a correction will account for very little improvement in the horizontal errors, especially the north-south direction error and could adversely impact the vertical error. For a receiver located in the southern hemisphere, the correction will further worsen the position error, especially in the north-south and vertical directions.

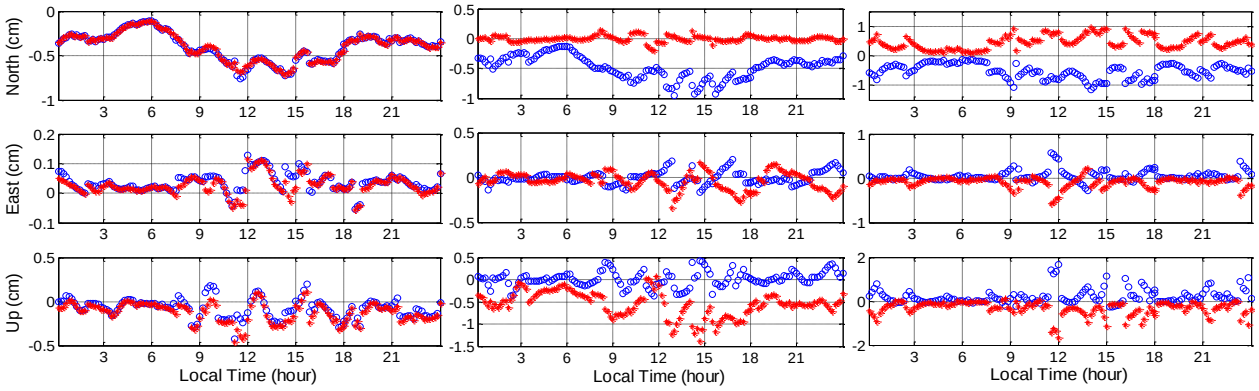

Arecibo, Puerto Rico Jicamarca, Peru Bahia Blanca, Argentina

Fig. 9. North, east, and vertical position errors resulting from the presence of a second order carrier phase error under two scenarios: the "*" correspond to the second order carrier phase errors computed by assuming that GPS signals can only propagate in the "X" mode, while the open circles result from considering both "X" and "O" modes of propagation, depending on the relative direction of the signal vector and of the B field.

1.2. Troposphere Error Modeling.

The troposphere conditions can be divided into two categories: nominal and non-nominal. For error propagation through the nominal troposphere, numerous models have been developed and these models are able to correct troposphere delays with cm-level accuracy [15]. For example, the modified Hopfield model (MHM) has been shown to accurately calculate both the hydrostatic (dry) and wet components of a nominal troposphere. A global 1-year data collection from June 1999 to March 2000 at 100 different sites shows that the global root-mean-square residual for the MHM hydrostatic zenith component is 1 cm, while the rms residual for the MHM wet zenith delay is 3 cm [15]. These results are relative to a total zenith delay of approx. 2.5 m. This means that the absolute MHM errors are approx 1% of the total delay. The MHM does not account for dispersive scattering delay due to propagation through rain, hail, or snow (hydrometeors). Propagation delay due to hydrometeors is dominated by heavy rain fall, and has been shown to be less than 1.5 cm/km for rain rates up to 20 cm/hour [16]. To gain a better understanding of the delays due to hydrometeors, GPS data from varying baseline lengths were analyzed in [17] and [18]. For a 16-km baseline, tropospheric delay differences of up to 0.4 m have been observed for satellite elevation angles above 12 degrees [17]. Over a 5-km baseline

length, tropospheric delay differences of up to 0.3 m have been observed for satellite elevations angles between 5 and 90 degrees [18]. To bound tropospheric decorrelation errors due to severe weather conditions, the MHM was used to simulate the worst case as shown in Fig. 10.

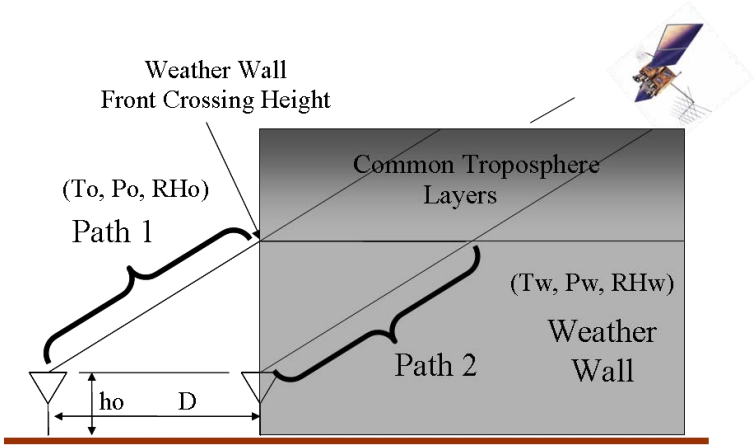

Fig. 10. Troposphere Model for Worst Case Spatial Decorrelation.

The MHM was used with nominal values for temperature, pressure and relative humidity (T_0, P_0, RH_0), while the conditions of a "weather wall" were calculated based on worst-case weather conditions (T_W, P_W, RH_W). The difference between the tropospheric propagation delays between two antennas separated by a distance D was then calculated. It was found that this methodology provides an overbound on the actual tropospheric spatial decorrelation error observed in actual data.

To extend the modeling of hydrometeors to a higher level of fidelity, additional information is required on the actual propagation path. Clearly, when all electromagnetic parameters are known, a complete solution can be calculated [19]. However, this method would not be practical as the tropospheric conditions in the presence of hydrometeors are only partially known. To obtain a model that can also be run efficiently for real-time corrections, a standard ray tracing approach was adopted for this research. First, two-dimensional weather radar data were obtained and tropospheric delays were modeled using the Vienna mapping function [20] with atmospheric parameters provided in [21]. The results were compared with measured propagation delay differences between two GPS receiver locations and are shown in Fig. 11. Good correlation is observed between the modeled and actual tropospheric delay differences between two locations near Rayleigh, North Carolina; RALR and NCRD which are part of the network of Continuously Operating Reference Stations (CORS). To enable a direct observation of the actual error, the GPS double differences (DD) are graphed, which are the propagation delay differences between two GPS satellites and two locations. DD processing removes the GPS receiver clock offsets and provides for a direct observation of the tropospheric differences. The model used for Fig. 11 assumes clouds and rain from an altitude of 300 m to 10,000 m, which enables the detection and prediction of tropospheric gradients, but does not account for the actual delays at the cm-level. Based on the findings of this research, the next step will be to use 3-dimensional (3D) weather radar data to further improve the propagation delay estimates.

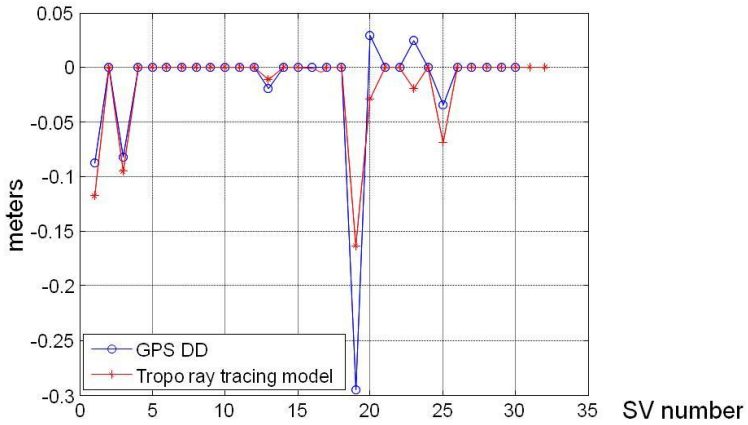

Fig. 11. Comparison of Ray Tracing with Actual GPS Measurements.

1.3. Satellite Orbit and Clock Error Studies.

Detailed analyses were performed for GPS satellite clock and orbit errors as they affect the performance of GPS range and receiver position measurements. Broadcast satellite orbit and clock data were compared with post-processed truth data from several data sources, including the National Geospatial-Intelligence Agency (NGA) and the International GNSS Service (IGS). Anomalies in the data were studied to determine their cause and verified using GPS receiver data. The focus has been on short-term satellite orbit and clock error growth performance to characterize how much error build-up will take place in between orbit and clock updates that are available every 15 minutes. Statistical distributions have been derived from archived data sets over three years. The analysis also addresses coasting performance after loss of precise clock and orbit updates. The data flow for the errors analysis is shown in Fig. 12.

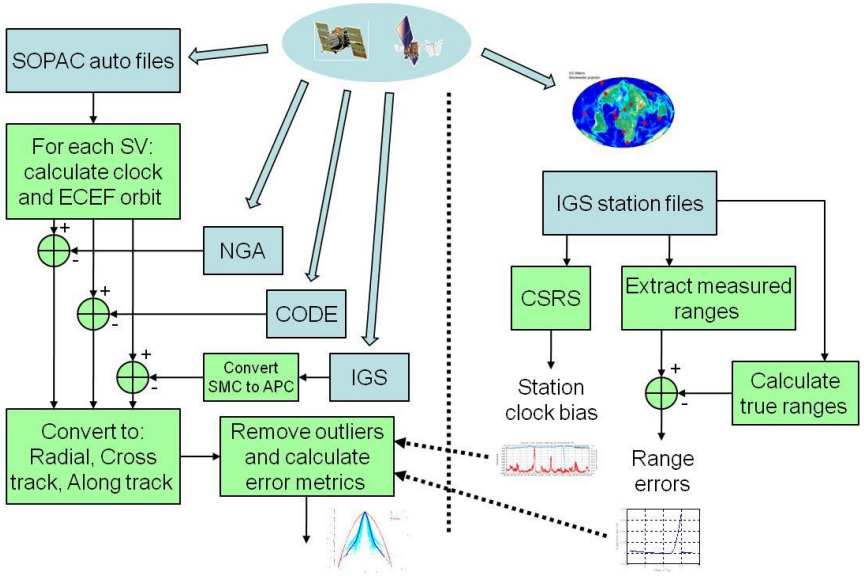

Fig. 12. Clock and Orbit Error Processing Data Flow.

Broadcast ephemerides are obtained from the Scripps Orbit and Permanent Array Center (SOPAC). Precise orbit and clock data from several sources was used: National Geospatial-Intelligence Agency (NGA), Center for Orbit Determination (CODE), and the International GNSS Service (IGS). Data from the latter organization is converted from the satellite mass center (SMC) to the antenna phase center (APC). Next, radial, cross track and along track errors are generated followed by an extensive validation process based on actual measurements from IGS station files processed by dedicated software as well as by independent solutions from the Canadian Spatial Reference System (CSRS).

After outlier removal and removal of satellite anomalies, distributions were calculated for seven error metrics: cross track (C), along track (A), radial (R), clock (cB), radial minus clock, 3D satellite position, and signal-in-space range error (SISRE) overbound. The SISRE overbound is calculated to determine the largest possible error under nominal conditions. The SISRE is calculated from: $\text{SISRE} = \text{R - cB} + \frac{1}{7} sign(\text{R - cB}) \sqrt{A^2 + B^2}$. Fig. 13 shows an example distribution graph for the SISRE for the Block IIA GPS satellites.

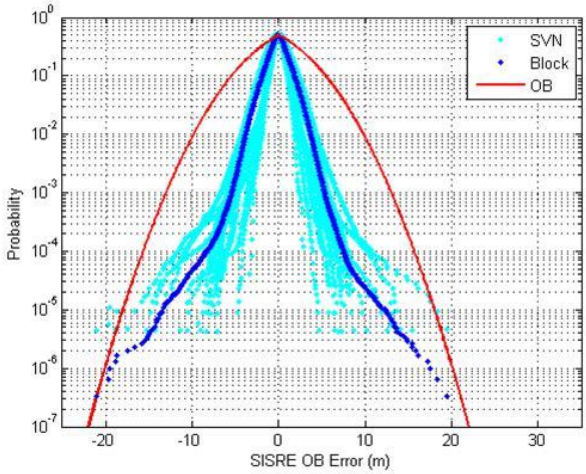

Fig. 13. Block IIA GPS Satellite SISRE Distributions.

The graph in Fig. 13 shows the cumulative distribution function (CDF) for values of the CDF less than or equal to 0.5 and shows 1-CDF for values of the CDF greater than 0.5. For this example, the standard deviation of SISRE is 1.51 m, while the Gaussian distribution that overbounds the tails of the CDF has a value of 4.22 m. Clearly, the SISRE error distribution does not follow a Gaussian distribution.

For systems that provide clock and orbit error corrections, the validity of the corrections is of great interest and can be evaluated by examining the statistics of the temporal error growth, provided by the changes in SISRE. Three operational scenarios must be considered: 1) Use the latest broadcast ephemeris; 2) Coast using a single ephemeris; and 3) Use the latest ephemeris with the transition between two sets of successive ephemerides made continuous. The three scenarios are necessary as the satellite clock and orbit broadcast changes nominally every hour. Example results are provided in Fig. 14 for Block IIA, Block IIR, and Block IIR-M satellites.

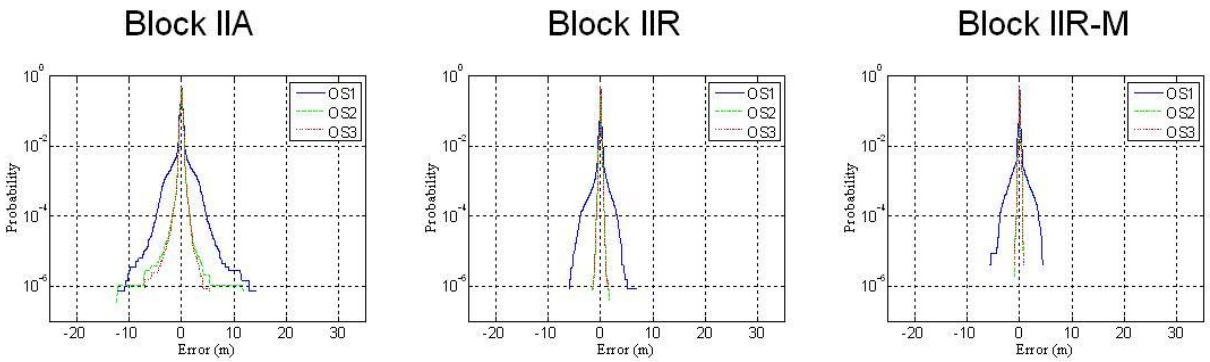

Fig. 14. Temporal SISRE Distributions for Different Satellite Block Types for 15-Minute Time Intervals.

From Fig. 14 it is observed that the standard deviation of the changes in SISRE over 15 minutes is 8 cm for the Block IIR-M satellites for operational scenario 3. Since the error growth is essentially linear over a 15-minute time interval, this corresponds to a temporal degradation of the combined satellite clock and orbit range errors of less than 0.1 mm/s.

References:

[1] Klobuchar, J., J. Kunches, "Comparative range delay and variability of the earth's troposphere and the ionosphere," *GPS Solutions*, DOI 10.1007/s10291-003-0047-5, 7, p.55-58, 2003.

[2] Basu, B., K. Groves, S. Basu, P. Sultan, "Specification and forecasting of scintillations in communication/navigaton links: current status and future plan," *J. Atmos. Solar-Terr Phy*., 64, p1745-1754, 2002.

[3] Fritsche, M., R. Dietrich, A. Rulke, M. Rothacher, R. Steigenberger, "Impact of higher-order ionosphere terms on GPS-derived global network solutions," Geophy. Res. Abstract, 7, 04735, 2005.

[4] Kedar, S., G. A. Hajj, B. D. Wilson, M. B. Heflin, "The effect of the second order GPS ionospheric correction on receiver positions," *Geophys. Res. Let*., 30(16), p.1829-1832, 2003.

[5] Brunner, F. K., and M. Gu, "An improved model for the dual frequency ionospheric correction of GPS observations," *Manuscripta Geodaetica*, 16, p.205-214, 1991.

[6] Datta-Barua, S., T. Walter, J. Blanch, and P. Enge, *Bounding high order ionosphere errors for the dual frequency GPS user*, Radio Science, 43, RS5010, doi:10.1029/2007RS003772, 2008.

[7] Hoque, M. M., N. Jakowski, "Mitigation of higher order ionospheric effects on GNSS users in Europe," *GPS Solutions*, DOI 10.1007/s10291-007-0069-5, 2007.

[8] Ratcliffe, J. A., The Magneto-ionic Theory and Its Applications to the Ionosphere, University Press, 1959.

[9] Morton, Y., Q. Zhou, F. van Graas, "Assessment of second order ionosphere error in GPS range observables using Arecibo incoherent scatter radar measurements," *Radio Sci.*, 44, RS1002, doi:10.1029/2008RS003888, 2009.

[10] Morton, Y., F. van Graas, Q. Zhou, J. Herdtner, "Assessment of the higher order ionosphere error on position solutions," *Navigation*, Vol.56, No.3, p185-193, Fall 2009.

[11] Matteo, N., and Y. Morton, "Ionosphere geomagnetic field: satellite observation and IGRF model comparisons," under revision for submission to *Adv. Space Research*.

[12] Matteo, N., Y. Morton, P. Chandrasekaran, F. van Graas, "Geographical Dependency of Higher Order Ionosphere Errors," *2009 ION GNSS Conference*, Savanna, GA, Sept. 2009.

[13] Bassiri, S., and G. A. Hajj, "High-order ionospheric effects on the global positioning system observables and means of modeling them," *Manuscripta Geodaetica*, vol.18, p.280-289, 1993.
[14] Morton, Y., R. Moore, and F. van Graas, "GPS signal propagation mode impact on receiver position errors," *2010 ION ITM*, San Diego, CA, Jan. 2010.
[15] Schüler, T., "On Ground-Based GPS Tropospheric Delay Estimation," Dissertation, Universität der Bundeswehr, München, Germany, 2001.
[16] Solheim, F. S., R. H. Ware and C. Rocken, "Propagation delays induced in GPS signals by dry air, water vapor, hydrometeors, and other particulates," *Journal of Geophysical Research*, Vol. 104, No. D8, pp. 9663–9670, April 27, 1999.
[17] Huang, J. and F. van Graas, "Comparison of Tropospheric Decorrelation Errors in the Presence of Severe Weather Conditions in Different Areas and Over Different Baselines," *Navigation*, Vol. 54, No. 3, 2007.
[18] Huang, J., F. van Graas, and C. Cohenour, "Characterization of Tropospheric Spatial Decorrelation Errors over a 5-km Baseline," *Navigation*, Vol. 55, No. 1, 2008.
[19] Chaubell, J., O. P. Bruno, and C. O. Ao, "Evaluation of EM-wave propagation in fully three-dimensional atmospheric refractive index distributions, "*Radio Sci.*, 44, RS1012, doi: 10.1029/2008RS003882, 2009.
[20] Boehm, J. and H. Shuh, "Vienna mapping function," Proceedings of the *16th National VLBI Meeting*, Leipzig, Germany, May 9-10, 2003.
[21] Lieve, H. J., "MPM – An atmospheric millimeter wave propagation model," *International Journal of Infrared and Millimeter Waves*, Vol.10:631-650, 1989.

2. Publications

- Published Journal Papers

[1] Morton, Y., F. van Graas, Q. Zhou, and J. Herdtner, "Assessment of the higher order ionosphere error on position solutions," *Navigation*, Vol.56, No.3, p185-193, Fall 2009.
[2] Morton, Y., Q. Zhou, and F. van Graas, "Assessment of second order ionosphere error in GPS range observables using Arecibo incoherent scatter radar measurements," *Radio Sci.*, Vol.44, RS1002, doi:10.1029/2008RS003888, 2009.

- Published Conference Papers

[1] Morton, Y., R. Moore, and F. van Graas, "GPS signal propagation mode impact on receiver position errors," *2010 ION ITM*, San Diego, CA, Jan. 2010.
[2] Matteo, N., Y. Morton, P. Chandrasekaran, F. van Graas, "Geographical Dependency of Higher Order Ionosphere Errors," *2009 ION GNSS Conference*, Savanna, GA, Sept. 2009.
[3] Morton, Y., F. van Graas, Q. Zhou, J. Herdtner, "Assessment of the Second Order Ionosphere Error on Position Solutions," *2008 ION GNSS*, Savanna, GA, Sept. 2008.
[4] Morton, Y., Q. Zhou, and F. van Graas, "Analysis of second order ionosphere error using incoherent scatter radar measurements," *Proc. 2008 Int. Ionosphere Effect Sym.*, Washington DC, May, 2008.

- Submitted Papers

[1] Moore, R. and Y. Morton, "Magneto-ionic polarization and GPS signal propagation," under revision for submission to *Radio Science*.
[2] Matteo, N., and Y. Morton, "Ionosphere geomagnetic field: satellite observation and IGRF model comparisons," under revision for submission to *Adv. Space Research*.
[3] Matteo, N., and Y. Morton, "Higher order ionosphere errors at Arecibo, Jicamarca, and Millstone Hills," under revision for submission to *Navigation*.
[4] Zhu, Z., P. Muvvala, and F. van Graas, "Troposphere Delay Modeling through Severe Weather Conditions using Radar Measurements," under revision for submission to *Navigation*.
[5] Cohenour, C., and F. van Graas, "GPS Orbit and Clock Error Distributions," provisionally accepted for publication in *Navigation*.
[6] Cohenour, C., and F. van Graas, "Temporal Decorrelation of GPS Range Measurements due to Satellite Orbit and Clock Errors," provisionally accepted for publication in *Navigation*.

3. Follow-On Uses

- Technology Assists
  - ✓ The data we used and the techniques we developed to compute the higher order ionosphere error were adapted by researchers at the Applied Physics Laboratory in Johns Hopkins University to assess the higher order ionosphere error in satellite-based radio occultation studies of the atmosphere.
  - ✓ We worked closely with AFRL-RYRN at Wright Patterson Air Force Base to support the WASPS Program by sharing our understanding and analysis of the higher order ionosphere error, troposphere error, multipath, and satellite orbit and clock errors.
  - ✓ Pre-prints of satellite clock and orbit error journal papers were provided to the Aerospace Corporation and Stanford University to support their investigations into GPS orbit and clock anomalies.

- Technology Transitions: None.

- Technology Transfers

  - ✓ Continued discussions with Holloman Air Force personnel on the use of the developed techniques in a future reference system.

4. Accomplishments and Successes

- Developed a new method to evaluate the higher order ionosphere using incoherent scatter radar and IGRF models. The method does not have to be concerned with any contaminations from other GPS range measurement errors sources.
- Obtained a massive archived electron density profiles at multiple sites. These data are excellent sources to characterize geographical, daily, seasonal, and solar activity dependency of the higher order error.
- Validated the IGRF model performance in ionosphere using multiple space-based instrumentation measurements over one decade period.
- Completed extensive higher order error characterization at high latitude, mid-low latitude, geomagnetic equatorial regions.

- Clarified the relationship between GPS signal polarization and its propagation mode through the ionosphere. Demonstrated the impact of prior mis-conception on higher order error correction effects.
- Compiled three years of detailed GPS satellite clock and orbit error statistics.
- Characterized GPS orbit and clock error performance both in an absolute sense and in a relative sense as a function of time.

5. Professional Personnel Supported

- Miami University Personnel

  Yu (Jade) Morton, Faculty
  Nick Matteo, Graduate Student
  Xiaolei Mao, Graduate Student

- Ohio University Personnel

  Frank van Graas, Faculty
  Curtis Cohenour, Research Engineer
  Zhen Zhu, Research Engineer
  Chen Chen, Graduate Student
  Rambabu Nalluri, Graduate Student
  Priyanka Muvvala, Graduate Student

6. Honors and Awards Received

- Yu Morton, Sigma Xi Researcher of the Year Award, Miami University, 2009.
- Nick Matteo, Institute of Navigation Graduate Award, 2009.

7. Professional Activities

Yu (Jade) Morton
- Outreach Chair, ION (2009)
- Eastern Region Member-At-Large, ION (2008)
- Chair, Bradley Parkinson Thesis Award Committee, ION (2008)
- Session Co-Chair, 2010 ION International Technical Meeting
- Session Co-Chair, 2009 ION Global Navigation Satellite Systems Conference
- Session Co-Chair, 2009 ION International Technical Meeting
- Focused Session Organizer, Advances in Positioning Sys., 2009 Int. Microwave Sym.
- Workshop Organizer, 2008 Miami ECE/ION Dayton Section Symposium
- Session Co-Chair, 2008 ION National Technical Meeting
- Award Committee Chair, 2008 New Navigation Tech. & Innovations Conf., Beijing, China
- Award Committee Chair, 2007 CPGPS China Forum, Guangzhou, China
- Technical Chair, 2007 ION Global Navigation Satellite Systems Conference
- Session Co-Chair, 2007 ION Annual Meeting
- Session Co-Chair, 2007 ION National Technical Meeting
- Editorial board, Springer journal GPS Solutions (since 2006)
- Associate Editor, IEEE Trans. Aerospace & Electronics (since 2008)

Frank van Graas

- Past President, ION (since 1999)
- Meetings Chair, ION (since 2002)
- Member Executive Board, IEEE/ION Position Location and Navigation Symposium (since 2005)
- Director, Consortium of Ohio Universities on Navigation and Timekeeping (since 2006)
- ION Executive Branch Science and Technology Policy Fellow (2008-2009)